Electronic Supplementary Material (ESI) for Journal of Materials Chemistry A

SUPPORTING INFORMATION

Fluorogenic detection of Tetryl and TNT explosives using nanoscopic-capped mesoporous hybrid materials

Yolanda Salinas, Alessandro Agostini, Edgar Pérez-Esteve, Ramón Martínez-Máñez, Félix Sancenón, M. Dolores Marcos, Juan Soto, Ana M. Costero, Salvador Gil, Margarita Parra and Pedro Amorós

Chemicals

The chemicals tetraethylorthosilicate (TEOS) (98%), *n*-cetyltrimethylammonium bromide (CTABr) (≥99 %), sodium hydroxide (≥98%), triethanolamine ($TEAH_3$) (≥99%), tris(2,2'-bipyridyl)dichlororuthenium(II) hexahydrate ($[Ru(bipy)_3]Cl_2 \cdot 6H_2O$) (100 %), 2,4-dinitrotoluene (2,4-DNT), *N*-methylaniline (98%) (NM), 2-nitrotoluene (NT), nitrobenzene (99%) (NB), thionyl chloride, 1-pyrenemethylamine hydrochloride, 4-pentynoic, 3-(azidopropyl)triethoxysilane, methylene blue and naphthalene were provided by Sigma-Aldrich and used as received. The 3% solution in acetonitrile of the subsequently nitrated explosives 2,4,6-trinitrophenylmethylnitramine (Tetryl), 2,4,6-trinitrotoluene (TNT), hexahydro-1,3,5-trinitro-1,3,5-triazine (RDX) and pentaerythritol tetranitrate (PETN) were purchased from SelectLab Chemicals. L-Ascorbic sodium salt (99%), potassium carbonate, sodium sulfate and cobalt (II) sulfate pentahydrate ($CuSO_4 \cdot 5H_2O$) were acquired from Scharlab (Barcelona, Spain). Analytical-grade solvents were purchased from Scharlab (Barcelona, Spain). All the reagents were used as received.

General Techniques

Powder XRD, TG analysis and N_2 adsorption-desorption techniques were employed to characterise the prepared materials. Fluorescence spectroscopy was used for studying the controlled release behaviour of the synthesised materials. The fluorescence measurements were carried out at 25°C. Powder X-ray diffraction measurements were taken in a Philips D8 Advance diffractometer using Cu K_α radiation. Thermo-gravimetric analyses were carried out on a TGA/SDTA 851e Mettler Toledo balance, using an oxidant atmosphere (air, 80 mL/min) with a heating programme consisting in a heating ramp of 10°C per minute from 293 K to 1273 K and an isothermal heating step at this temperature for 30 minutes. N_2 adsorption-desorption isotherms were recorded with a Micromeritics ASAP2010 automated sorption analyser. Samples were degassed at 120°C in vacuum overnight. Specific surface areas were calculated from the adsorption data in the low pressures range using the BET model. Pore size was determined following the BJH method. The size distribution of particle dispersions was measured with a Malvern Masterisizer 2000 (Malvern, UK) using acetonitrile as dispersant. For

data evaluation, an optical model based on the Mie theory was created using the instrumental software assuming 1.45 as the real and 0.001 as the imaginary part of the refractive index of the particles. Results given are the mean of 5 successive measurements. Fluorescence spectroscopy was carried out with a Felix 32 Analysis Version 1.2 (Build 56) PTI (Photon Technology International). TEM images were obtained with a 100 kV Philips CM10 microscope. ^{1}H and ^{13}C nuclear magnetic resonance (NMR) were acquired with a Varian 300 spectrometer (Sunnyvale, CA, USA) and the Mass spectrometry analysis was performed employing a MALDI TOF/TOF 4700 Proteomics Analyser from Applied Biosystems.

Synthesis

Synthesis of 4-pentynoyl chloride: Thionyl chloride (410 μL, 5.6 mmol) was added to a solution of 4-pentynoic acid (500 mg, 5.1 mmol) in benzene (5 mL) in an argon atmosphere. The reaction was stirred at room temperature for 4 hours and for 1 additional hour at reflux. The benzene and the excess of thionyl chloride were eliminated in a rotary evaporator. Finally, 4-pentynolyl chloride was taken up in THF (5 mL) and the solution used in the next step of the synthetic sequence.

*Synthesis of compound **1***: 1-Pyrenemethylamine hydrochloride (500 mg) was dissolved in basic water and then extracted with diethyl ether in order to obtain the free base 1-pyrenemethylamine. The ether layer was then dried (Na_2SO_4), filtered and the solvent removed by rotary evaporation. The resulting yellow solid was used to prepare pyrene derivative **1**. Next, 1-pyrenemethylamine (200 mg, 0.75 mmol) was dissolved in benzene (25 mL) and then an excess of dry K_2CO_3 was added. The 4-pentynoyl chloride solution (2.5 mL) was added to the suspension and the resulting yellow crude was stirred overnight at room temperature (see Figure SI-1). The benzene and THF in the crude reaction were removed by rotary evaporation and the crude was suspended in ethyl acetate (20 mL). The organic phase was washed with basic water (in order to hydrolise unreacted thionyl chloride and 4-pentynoyl chloride), with distilled water, and finally, with acidic water until a neutral pH was obtained. The organic layer was then dried (Na_2SO_4), filtered and the solvent was removed by rotary evaporation. Final product **1** was obtained as a yellow solid (187 mg, 0.60 mmol, 80.5% yield). The final structure of **1** was confirmed by ^{1}H-NMR, ^{13}C-NMR and mass spectra measurements.

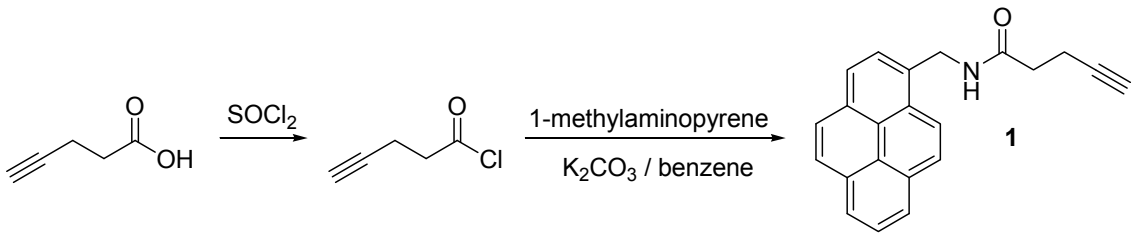

Figure SI-1. Synthesis of compound **1**.

^{1}H-NMR (300 Mhz, $CDCl_3$) δ: 1.91 (s, 1H, C≡C-**H**), 2.43 (t, 2H, C**H$_2$**-C≡C-H), 2.57 (t, 2H, C**H$_2$**-CH_2-C≡C-H), 5.16 (s, 2H, Pyr-C**H$_2$**-N), 5.92 (br s, 1H, CO-N**H**), 7.96-8.26 (m, 9H, **Pyr**) ppm. ^{13}C-NMR (75 Mhz, $CDCl_3$) δ: 15.0, 35.5, 42.1, 69.4, 82.9, 122.8, 124.8, 125.1, 125.4, 126.1, 127.2, 127.3, 127.6, 128.3, 129.1, 130.8, 130.9, 131.1, 170.5. HRMS-EI *m/z* calculated for $C_{22}H_{17}NO$ 311.1310, measured for MH^+ 312.1338.

Synthesis of the mesoporous silica support: The molar ratio of the reagents in the mother liquor was fixed to 7 $TEAH_3$: 2 TEOS: 0.52 CTABr: 0.5 NaOH: 8.89 H_2O. In a typical synthesis leading to the MCM-41 pure silica, CTABr (4.67 g) was added at 118°C to a $TEAH_3$ solution (25.76 g) containing NaOH (0.012 mol) and a silatrane derivative (e.g., 0.049 mol, 11 mL of TEOS) was added at 70°C to $TEAH_3$, e.g., in the form of Si(TEA)($TEAH_2$), where TEA was the fully deprotonated ligand). Then deionised water (80 mL) was added with vigorous stirring at 70°C. After some minutes, a white suspension was obtained. This mixture was aged at room temperature overnight. The resulting powder was collected by filtration and washed with water until pH 6-7. Finally the solid was dried at 70°C (MCM-41 as synthesised). To prepare the final porous material (MCM-41), the as-synthesised solid was calcined at 550°C for 5 h to remove the template.

*Synthesis of solid **S1***: In a typical synthesis, template-free MCM-41 (3 g) and $[Ru(bipy)_3]Cl_2{\cdot}6H_2O$ (1.8 g, 2.4 mmol) were suspended in acetonitrile (120 mL) in a round-bottomed flask. To remove the adsorbed water, 40 mL of acetonitrile were distilled using a Dean-Stark set-up. Then, the mixture was stirred for 24 hours at room temperature for the purpose of achieving maximum loading in the pores of the MCM-41 scaffolding. Afterwards an excess of 3-(azidopropyl)triethoxysilane (1.48 mL, 6 mmol) was added, and the suspension was stirred for 5.5 h. Finally, the orange-yellow solid was filtered off. In a second step, the mixture of azide-functionalised microparticles (3 g) and pyrene derivative **1** (303.23 mg, 0.975 mmol) was suspended in 50:50 v/v DMSO-water (100 mL) in the presence of an excess of the ruthenium (II) dye (1.8 g, 2.4 mmol) in order to avoid the delivery of the dye from the pores to the bulk solution during the synthesis of this solid. Then, a solution of $CuSO_4{\cdot}5H_2O$ 1.0 x 10^{-3} mol dm^{-3} (9.75 mL) and sodium ascorbate (19.32 mg, 0.097 mmol) was added. The reaction mixture was stirred at room temperature for 3 days. Microparticles were filtered off and washed with CH_2Cl_2 (100 mL), H_2O (100 mL), acetonitrile (100 mL), THF (250 mL) and dried at 70°C for 12 h.

Material Characterisation

MCM-41 as-synthesised, calcined MCM-41 and **S1** materials were characterised by standard techniques. Figure SI-2 shows the powder X-ray patterns of the solid MCM-41 as-synthesised (without calcination), calcined MCM-41 and **S1**. The powder XRD of siliceous MCM-41 as-synthesised shows four low-angle reflections that are typical of the hexagonal-ordered array which can be indexed as (100), (110), (200), and (210) Bragg peaks. A significant shift of the (100) reflection and a broadening of the (110) and (200) peaks in the XRD powder of the MCM-41 calcined sample are clearly seen. This scenario corresponds to an approximate cell contraction of ca. 6-8 Å during the calcination step. Despite this clear partial order loss, the fact that the overlapped (100) and (200) reflections are observed indicates that a certain

relative mesopore symmetry is preserved after calcination. Figure SI-2 also shows the curve that corresponds to **S1**. For this solid, reflections (110) and (200) were lost, most probably relating to a reduced contrast because of the pore voids filling with the ruthenium complex. Nevertheless, the clear presence of the (100) peak in this pattern suggests that the loading process with the $[Ru(bipy)_3]^{2+}$ complex, and the additional functionalisation with 3-(azidopropyl)triethoxysilane and pyrene derivative **1**, have not substantially modified the mesoporous MCM-41 support.

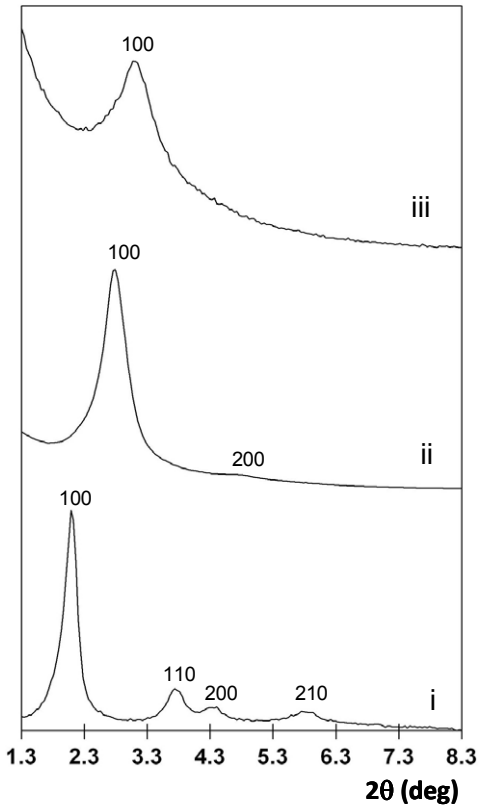

Figure SI-2. Powder X-Ray diffractograms showing the X-Ray patterns of the MCM-41 scaffolding as synthesized (i), MCM-41 after the calcination process (ii) and final solid **S1** (iii).

The presence of the mesoporous structure in the final functionalised solid (**S1**) was also confirmed by the TEM analysis, in which the typical channels of the MCM-41 matrix were visualised as alternate black and white stripes (see Figure S1-3 for solid **S1**). The figure also shows that the prepared **S1** was obtained as microparticles. The TEM images also indicate that the loading and grafting procedures did not modify the mesoporous structure of the starting material.

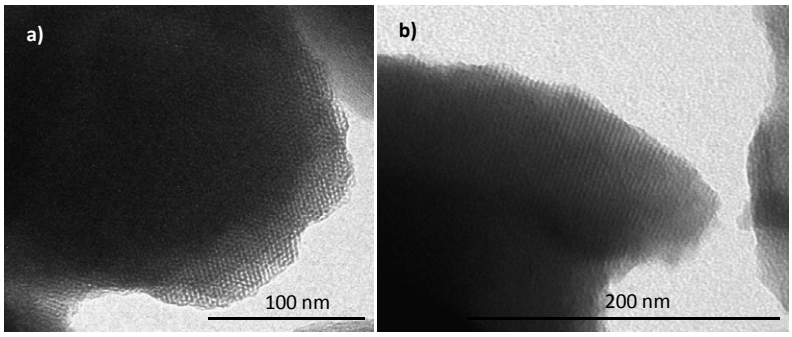

Figure SI-3. TEM image of a) the MCM-41 solid support and b) solid **S1**, showing the typical hexagonal porosity of the MCM-41 matrix.

LD (Laser Diffraction) studies showed **S1** microparticles with a mean diameter of 30.2 μm (see Figure SI-4). The studies also shown that the size of the microparticles was not modified throughout the loading and functionalization processes.

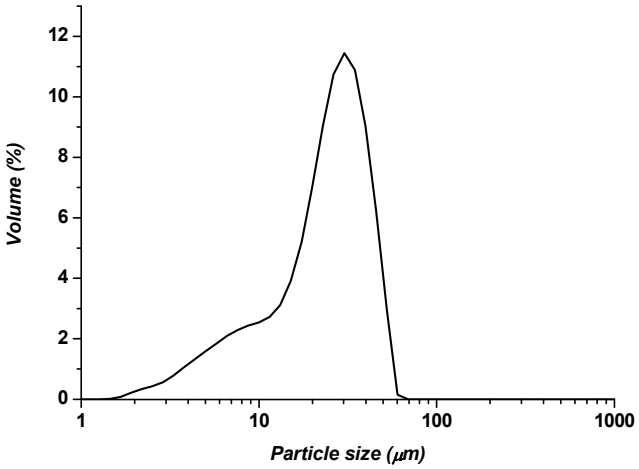

Figure SI-4. Statistical representation of particle size obtained by LD (Laser Diffraction) studies. The average size of **S1** microparticles was found to be 30.2 μm.

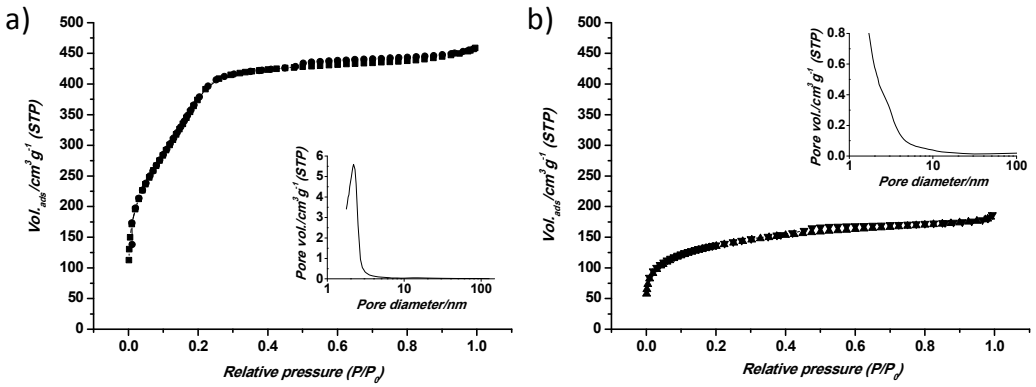

Figure SI-5. The nitrogen adsorption-desorption isotherms for (a) the MCM-41 mesoporous material (b) **S1**.

The N_2 adsorption-desorption isotherms of the MCM-41 calcined material show a typical curve for these mesoporous solids; i.e., an adsorption step at the intermediate P/P_0 value (0.2-0.4). This curve corresponds to a type IV isotherm, in which the observed step may be related to the nitrogen condensation inside the mesopores by capillarity (see Figure SI-5). The application of the BET model resulted in a total specific surface value of 1415 m^2/g. From the XRD, porosimetry and TEM studies, the a_0 cell parameter (3.64 nm), the pore diameter (2.29 nm) and a value for the wall thickness of 1.35 nm can be calculated. The N_2 adsorption-desorption isotherms of **S1** (see Figure SI-4) are typical of mesoporous systems with filled mesopores, and a significant decrease in the N_2 volume adsorbed is observed. In fact, these solids present flat curves when compared (on the same scale) to those of the MCM-41 parent material, indicating significant pore blocking and the subsequent absence of appreciable porosity. This is an expected result if we bear in mind that these solids have a high content of dye filling pores. The specific surface values, pore volumes and pore sizes for MCM-41 and **S1** are presented in Table SI-1.

Table SI-1. The BET-specific surface values, pore volumes and pore sizes calculated from the N_2 adsorption-desorption isotherms for selected materials.

	S_{BET} ($m^2\ g^{-1}$)	Pore Volume [a] ($cm^3\ g^{-1}$)	Pore size [a] (nm)
MCM-41	1415	0.88	2.29
S1	484.3	0.21	-

[a] Volume (V) and diameter (D) of the mesopores.

The content of the $[Ru(bipy)_3]^{2+}$ complex and the pyrene derivative in the prepared solid **S1** were determined by thermogravimetric measurements, and amount to 0.061 mmol/g SiO_2 and 0.104 mmol/g SiO_2, respectively. The heating ramp used to perform the thermogravimetric analyses consisted in a heating ramp of 10°C per minute, from 120°C to 1000°C, and an isothermal step at this temperature for 30 minutes. Examination of the thermogravimetric curve and its first derivative shows four weight loss steps: a first weight loss of 11.50% corresponding to solvents elimination ($T < 200$°C); a second weight loss of 9.73% due to the decomposition of the organic groups anchored on the siliceous surface ($200 < T < 360$°C); a third weight loss of 2.47% assigned to the decomposition of the ruthenium complex ($360 < T < 800$°C); finally, a weight loss of 0.87% owing to the condensation of the silanols on the siliceous surface ($T > 800$°C).

The higher amount of pyrene (0.104 mmol/g SiO_2), when compared with the ruthenium dye (0.061 mmol/g SiO_2), is a direct consequence of the low yield (about 40%) of the click reaction used for the grafting of the fluorophore. Bearing this in mind, there are pores without a sufficient amount of pyrene groups in their surroundings that are unable to retain the ruthenium complex. After the click reaction solid **S1** was exhaustively washed with dichloromethane, water, acetonitrile and tetrahydrofuran in order to remove the adsorbed matter and the ruthenium dye

from the non-closed pores (with the aim to achieve a "zero release" material). This fact accounts for the specific surface presented by **S1** (484.3 m^2 g^{-1}) and also for the apparent contradiction that there are more pyrene anchored in the outer surface than ruthenium complex in the inner of the pores.

Solvent selection

The studies into the explosive-induced uncapping paradigm were carried out in acetonitrile. In this solvent, a remarkably rather tight pore closure was observed and, at the same time, both the ruthenium dye and the selected explosives showed suitable solubility. Protic solvents (such as methanol and ethanol) are avoided because could give certain charge-transfer interactions with the electron deficient nitroaromatic compounds. Moreover water acetonitrile mixtures were also tested but unfortunately in this media no sensing features were observed when using **S1**.

Fluorescence quenching studies

To confirm the fact that the observed response of solid **S1** arises from the interaction between the anchored pyrene and nitroaromatic explosives TNT and Tetryl, further fluorescence measurements were taken (at 25°C). Indeed, 1 mg of **S1** was suspended in 3 mL of the acetonitrile solutions of TNT and Tetryl (2.0 x 10^{-3} mol dm^{-3}), while the emission of pyrene (excitation at 341 nm) was measured in the presence of increasing quantities of the nitroaromatic explosives. As seen in Figure SI-6, the monomer emission of the appended pyrene was quenched upon addition of nitroaromatic explosives.

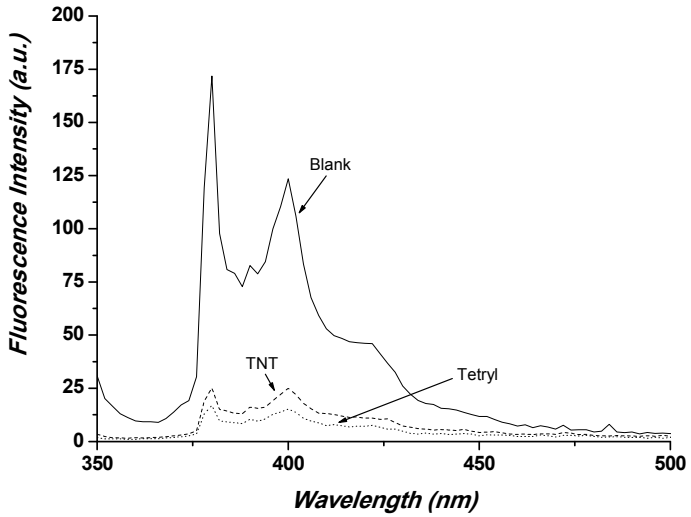

Figure SI-6. The fluorescence spectrum of the acetonitrile suspensions of **S1** (at 25°C) in the presence of TNT and Tetryl (2.0 x 10^{-3} mol dm^{-3}).

Sterm and Volmer considered the quenching process to be a bimolecular reaction which competes with the radiative process and all other molecular processes. Following this, we measured the quenching constants of the grafted pyrene with Tetryl and TNT. The procedure followed is analogous to that described in the dye release studies. Briefly, 4 mg of **S1** were suspended in 10 mL of an acetonitrile containing explosives TNT or Tetryl. Different aliquots (3

mL) were taken after 1 min of reaction, and the emission of the appended pyrene was measured. The Stern-Volmer plots of relative fluorescence intensity (F_0/F) of **S1** versus Tetryl and TNT concentration are shown in Figure SI-7 in which F_0 and F are the fluorescence intensity of the hybrid material before and after adding explosive, respectively. It is notable that the F_0/F versus [explosive] plots bends upwards instead of being linear, which may be due to the pyrene emission is quenched by a static quenching or with the participation of a dynamic quenching. The Stern-Volmer curves of **S1** in acetonitrile can be well fitted to the exponential equations $F_0/F=1.13e^{1617[Tetryl]}$ and $F_0/F=1.14e^{1166[TNT]}$ with quenching constants (in the low concentration range) of about 3044 M^{-1} and 1050 M^{-1} for Tetryl and TNT, respectively.

The values of the Stern-Volmer quenching constants clearly indicate that Tetryl is able to provide the strongest interactions with the pyrene grafted on the surface of the **S1** material. This is most likely related to the more electron-deficient character of Tetryl when compared with TNT. The Stern-Volmer quenching constants measured for **S1** were of the same order of magnitude as those measured for either polymeric materials or molecular fluorophores in the presence of nitroaromatic molecules.

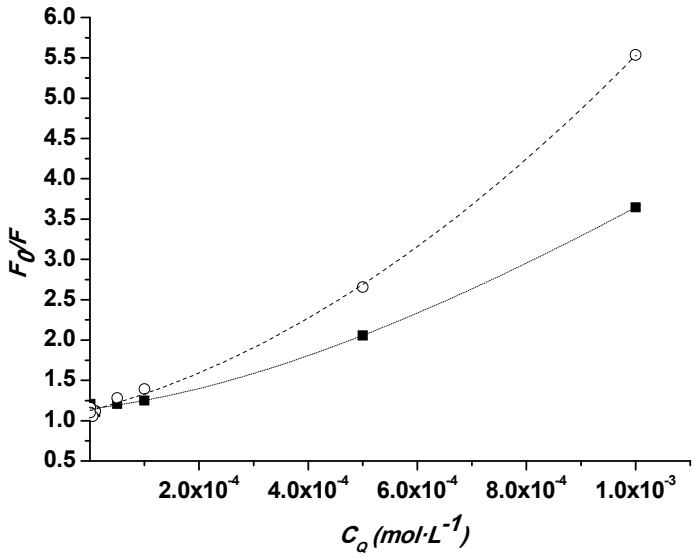

Figure SI-7. A Stern-Volmer quenching representation for acetronitrile suspensions of **S1** upon addition of Tetryl (o) and TNT (■).

Dye release studies

For the dye release studies (carried out at 25°C), 4 mg of **S1** were suspended in 10 mL of acetonitrile solution (2.0×10^{-3} mol dm^{-3}) of the following compounds: 2,4-DNT, TNT, Tetryl, hexahydro-1,3,5-trinitro-1,3,5-triazine (RDX), pentaerythritol tetranitrate (PETN), *N*-methylaniline (NM), 2-nitrotoluene (NT), nitrobenzene (NB), methyelene blue (MB) and naphthalenene (NP). Different aliquots (2 mL) were separated and filtered after 10 minutes. The delivery of the dye from the pore voids to the solution was monitored by the emission band of the $[Ru(bipy)_3]^{2+}$ complex centred at 625 nm. The results are observed in Figure 3 (see

the manuscript). Of all the nitroaromatic derivatives tested, only Tetryl and TNT were able to uncap the pores with the subsequent release of the ruthenium complex.

Ratiometric sensing measurements

For ratiometric sensing studies, 1 mg of **S1** was suspended in 3 mL of the acetonitrile and the emission spectra, upon excitation at 341 nm, registered. Suspensions of **S1** alone showed the typical broad structured pyrene monomer emission in the 370-450 nm range. Addition of increasing quantities of TNT and Tetryl, to **S1** suspensions, induced a gradual quenching of the pyrene monomer emission together with the appearance of a new fluorescence centred at 625 nm (due to the ruthenium complex released upon gate opening). Figure SI-8 showed the emission changes observed for acetonitrile **S1** suspensions upon addition of increasing quantities of TNT (nearly the same response was obtained upon addition of Tetryl).

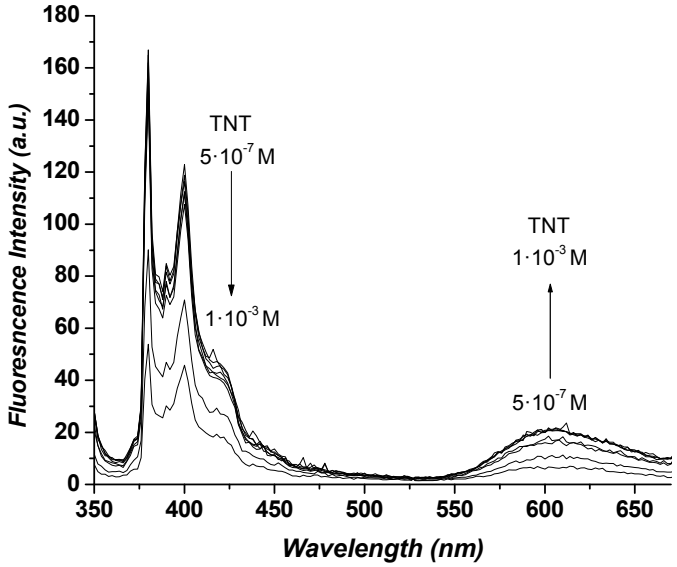

Figure SI-8. Emission changes of **S1** acetonitrile suspensions (at 25°C) upon addition of increasing quantities of TNT (excitation at 341 nm).

Limits of detection studies

The limits of detection using **S1** for TNT and Tetryl were determined using 4 mg of solid **S1**, which were suspended in 10 mL of the different solutions containing increasing concentrations of the corresponding explosive (at 25°C). Different aliquots (2 mL) were taken up and filtered after 10 minutes. The delivery of the $[Ru(bipy)_3]^{2+}$ complex from the pore voids to the solution was easily monitored by the emission band at 625 nm (see Figure SI-9).

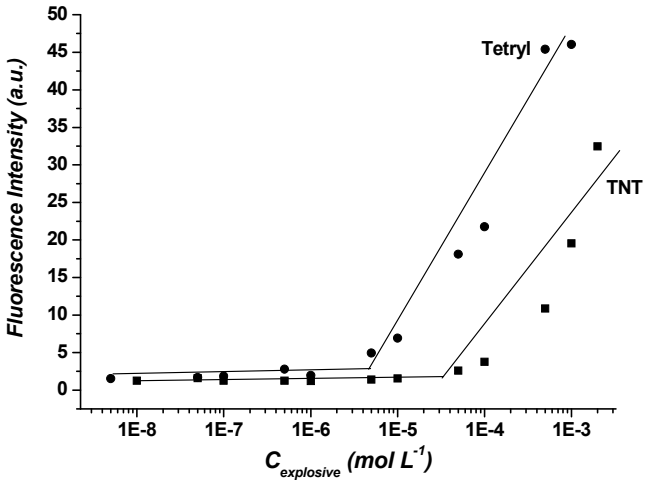

Figure SI-9. Calibration curves obtained from the acetonitrile suspensions of **S1** (at 25°C) upon addition of increasing quantities of TNT and Tetryl (excitation at 451 nm, emission at 625 nm).

The fluorimetric titrations, shown in Figure SI-9, allowed us to determine the limits of detection for Tetryl (1.4 ppm) and TNT (11.4 ppm). The detection limits for Tetryl and TNT using solid **S1** were also determined by monitoring the nitroaromatic-induced pyrene quenching. In particular, 4 mg of solid **S1** were suspended in 10 mL of the different solutions containing increasing concentrations of the corresponding explosive. Different aliquots (2 mL) were taken up after 10 minutes. The quenching delivery of the appended pyrene was easily monitored by the monomer emission bands in the 370-440 nm range (see Figures SI-10 and SI-11). The fluorimetric titrations allowed us to determine the limits of detection for Tetryl (8.6 ppm) and TNT (9.1 ppm).

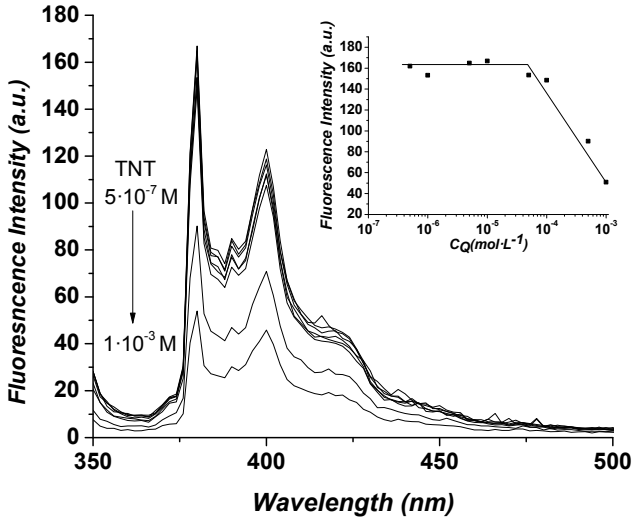

Figure SI-10. Quenching of the grafted pyrene upon addition of increasing quantities of TNT to acetonitrile suspensions of **S1** (at 25°C). The inset shows the calibration curves obtained from the acetonitrile suspensions of **S1** upon addition of increasing quantities of TNT (excitation at 341 nm, emission at 380 nm).

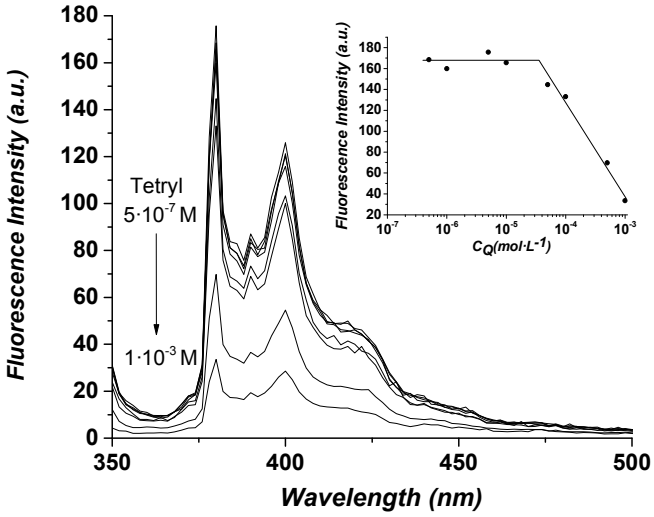

Figure SI-11. Quenching of the grafted pyrene upon addition of increasing quantities of Tetryl to acetonitrile suspensions of **S1** (at 25°C). The inset shows the calibration curves obtained from the acetonitrile suspensions of **S1** upon addition of increasing quantities of Tetryl (excitation at 341 nm, emission at 380 nm).

Gating mechanism

The experimental evidences, no pyrene excimer emission in acetonitrile and in water was observed, pointed to an alternative mechanism rather than to a simple pyrene-pyrene interaction. At this respect, the high quantity of pyrene grafted in the outer of the pores (0.104 mmol/g SiO_2) pointed toward the formation of a relatively dense monolayer around the pores that inhibited the release of the entrapped ruthenium complex. Bearing in mind an external surface area of 29 m^2 g^{-1} (for the solid with the pores loaded with ruthenium complex and the azide moiety grafted in the outer surface) and applying the equation (1):

$$\beta_A = \alpha_A \times 10^{-3} \times S^{-1} \times 10^{-18} \times N_A \quad (1)$$

where α_A is the mmol of pyrene derivative/ g solid in **S1**, S is the external surface area and N_A is the Avogadro's number, an average distance between pyrene molecules of 7.8 Å was estimated. With an average pore diameter of 2.29 nm and an a_0 cell parameter of 3.64 nm we can estimate that each pore was surrounded by 10 pyrene molecules. This leads to the formation of a dense pyrene network around the pore outlets that inhibit cargo release. Also the molecule that acts as gate is composed by a pyrene fluorophore (electron donor character) and by a 1,2,3-triazole heterocycle (electron acceptor character). As a consequence, a charge-transfer process, in the pyrene-triazole molecule, is active leading to the generation of a strong dipole moment (of 3.2 D estimated through quantum mechanical calculations at the semi-empirical level using Hyperchem 6.0 software). Bearing in mind this fact, strong dipole-dipole interactions between the gating molecules would be active in **S1** and most likely accounted for the inhibition of the cargo release observed. The nitroaromatic explosives (Tetryl and TNT) added could give charge-transfer interactions, with the grafted pyrene subunits inhibiting the dipole-dipole interaction and therefore inducing a reduction of the steric crowding around the

pore outlets and the disruption of the dipole-dipole forces. As a consequence a release of the entrapped ruthenium complex was observed.

Moreover, in order to discard a possible nitroaromatic-induced displacement of the ruthenium complex due to the diffusion of nitroaromatics into the pores several experiences were carried out. At this respect, the chromogenic response in the presence of Tetryl and TNT of a hybrid solid that contains the ruthenium complex, in the inner of the pores, and azide moieties, in the external surface, has been tested. For that, 4 mg of solid were suspended in acetonitrile (10 mL) or in acetonitrile containing Tetryl or TNT (10 mL, 2.0 x 10^{-3} mol dm^{-3}). The suspensions were stirred for 10 minutes and then filtered. Then, the absorption or the emission band of the ruthenium complex released was measured. The same absorbance (see Figure SI-12) and emission intensity for the solid alone or solid in the presence of Tetryl and TNT was obtained indicating that there are no displacement of ruthenium complex by the nitroaromatic explosives.

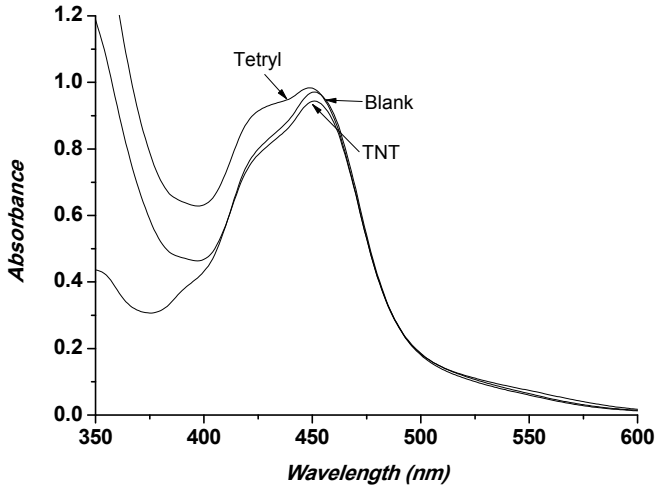

Figure SI-12. Absorbance of acetonitrile suspensions of a solid that contains the ruthenium complex (in the inner of the pores) and azide moieties (in the external surface) in the absence and in the presence of Tetryl and TNT (2.0 x 10^{-3} mol dm^{-3}).